

# Delay of Regeneration by Adding Aluminum in Boron-Doped Crystalline Si

Melanie Mehler,\* Andreas Schmid, Annika Zuschlag, Matthias Trempa, and Giso Hahn

Here, two B-doped Cz-grown Si materials with different Al concentrations are investigated concerning the long-term behavior of excess charge carrier lifetime under injection at elevated temperature. By determining the defect density and the surface saturation current density, a delay in regeneration and a delay in the onset of surface-related degradation is found in the material containing an order of magnitude more Al. Investigations under constant excess carrier concentration reveal that the effect of the delay is still significant, but less pronounced compared with constant generation conditions, so the effect causing the delay seems to be injection dependent. The findings can be explained by the higher activation energy for the splitting of Al–H pairs compared with splitting of B–H pairs, which might cause a delayed release in H from the dopant H configuration. Assuming that regeneration depends on this released H, the delay in regeneration can be explained by this model.

(LeTID).<sup>[8,9]</sup> As for BO-LID, a regeneration phase can be observed for LeTID after maximum degradation. Unlike for BO-LID there is no clear scaling of degradation strength with oxygen or doping concentration for LeTID.<sup>[9]</sup> In various studies, the root cause and influencing factors of LeTID have been investigated. It could be shown that LeTID strength and kinetics depend on various external parameters such as treatment temperature,<sup>[9,10]</sup> the excess charge carrier concentration (or injection),<sup>[9]</sup> and the hydrogen content in the dielectric passivation layer.<sup>[11–13]</sup> A clear dependency of LeTID strength on peak firing temperature and cool-down ramp,<sup>[14–16]</sup> as well as wafer thickness, could be observed.<sup>[17]</sup> A gettering step and the local defect structure can have an effect on

## 1. Introduction

Different degradation phenomena exist that affect the efficiency of multicrystalline (mc) and Czochralski-grown (Cz) silicon solar cells due to a decrease in lifetime of generated excess charge carriers. One example is light-induced degradation (LID), which often occurs due to interaction of boron and oxygen, also referred to as BO-LID.<sup>[1–4]</sup> For the BO-LID phenomenon, there exists also a mechanism that increases the lifetime to its original high starting value (referred to as regeneration) due to injection of excess charge carriers and the presence of hydrogen in the Si bulk.<sup>[5–7]</sup>

Another degradation phenomenon, which was discovered in 2012, is the light- and elevated temperature-induced degradation

LeTID,<sup>[17]</sup> although this effect cannot be observed to the same extent in all Si materials. In recent studies the occurrence of the LeTID defect could be related to the presence of hydrogen in silicon bulk, with higher concentration of H leading to more pronounced degradation and a higher defect density.<sup>[18–20]</sup>

In addition to these influencing factors, metal impurities might be involved in the LeTID process.<sup>[14,21,22]</sup> According to Wagner et al.,<sup>[23]</sup> the strength of LeTID degradation of Cz passivated emitter and rear cell (PERC) solar cells seems to correlate with the aluminum concentration in the Cz wafer, as investigated by correlating cell parameters directly after firing with the values after 1 week of treatment time at 75 °C and 0.5 suns illumination. Therefore, it can be concluded that Al might be involved in the responsible LeTID defect.


To further investigate the influence of Al in the Si bulk on LeTID, this study considers two boron-doped Cz-Si materials with different Al concentrations and its effect on the degradation and regeneration kinetics. As the strength of the LeTID effect strongly depends on the firing temperature,<sup>[14,24]</sup> two different firing temperatures are considered. In addition to that, the influence of a gettering step is investigated. As various defect reaction rates depend on the injection level, which does not remain constant under constant illumination over time due to the changing lifetime,<sup>[25]</sup> the investigation of the long-term lifetime behavior is additionally conducted under constant excess carrier concentration conditions.

## 2. Experimental Section

For the investigation, B-doped and B + Al co-doped Cz-grown Si wafers (in the following referred to as “B-Reference” and

M. Mehler, A. Schmid, A. Zuschlag, G. Hahn  
Department of Physics  
University of Konstanz  
78457 Konstanz, Germany  
E-mail: melanie.mehler@uni-konstanz.de

M. Trempa  
Fraunhofer Institute for Integrated Systems and Device Technology  
Schottkystraße 10, 91058 Erlangen, Germany

 The ORCID identification number(s) for the author(s) of this article can be found under <https://doi.org/10.1002/pssa.202100603>.

© 2021 The Authors. physica status solidi (a) applications and materials science published by Wiley-VCH GmbH. This is an open access article under the terms of the Creative Commons Attribution-NonCommercial License, which permits use, distribution and reproduction in any medium, provided the original work is properly cited and is not used for commercial purposes.

DOI: 10.1002/pssa.202100603

“B + Al,” respectively) served as the base material with bulk resistivity of  $\approx 1.2 \Omega \text{ cm}$  for the B-Reference and  $\approx 1.3 \Omega \text{ cm}$  for B + Al. According to secondary-ion mass spectrometry (SIMS) measurements, both doped materials contained very similar amounts of boron ( $\approx 1 \times 10^{16} \text{ at cm}^{-3}$ ). During crystallization of the B + Al co-doped material, deliberate addition of aluminum led to an Al concentration in the investigated samples that was one order of magnitude higher ( $\approx 3 \times 10^{14} \text{ at cm}^{-3}$ ) than for the B-Reference ( $\approx 4 \times 10^{13} \text{ at cm}^{-3}$ ). Thus, the boron concentration was still dominant and mainly indicated the base resistivity in the case of B + Al. Al in the B-Reference stemmed from an unintentional background contamination, whereas in B + Al material, the extra Al content was added intentionally. The Cz-Si material was grown in an industrial-sized Cz furnace at a partner company site. The complete data of SIMS measurements of the dopants and Fourier-transform infrared spectroscopy (FTIR) measurements of the interstitial oxygen concentrations  $[\text{O}_i]$  (according to SEMI MF1188) for the respective materials are shown in Table 1.

For the degradation experiments,  $5 \times 5 \text{ cm}^2$  samples were lasered from  $156 \times 156 \text{ mm}^2$  Cz-Si wafers. The saw damage was removed from all samples by etching in KOH. To allow a comparison between gettered and non-gettered samples, one-half of the samples received after Piranha and ozone cleaning a  $\text{POCl}_3$ -based emitter ( $\approx 55 \Omega \text{ sq}^{-1}$ ), which was removed in the subsequent etching step (“gettered” samples). For the formation of the emitter,  $\text{POCl}_3$  diffusion at  $837^\circ \text{C}$  was conducted. The other half of the samples (“non-gettered”) was etched to the same thickness as the gettered ones, so that during firing, the temperature–time profile was the same for all samples. After an additional Piranha and ozone-cleaning step, all samples received on the front and back side a  $75 \text{ nm SiN}_x\text{:H}$  layer by plasma-enhanced chemical vapor deposition (PECVD) as surface passivation (direct PECVD tool from centrotherm). One half of the samples was fired in a belt furnace at a set peak temperature  $T_{\text{set,peak}} = 750^\circ \text{C}$  and the other half at  $T_{\text{set,peak}} = 850^\circ \text{C}$ . The actual temperature of the samples was determined with a temperature tracker DQ1860 from Datapaq in combination with a type-k thermocouple from Omega. The measured actual peak temperatures were  $20\text{--}30^\circ \text{C}$  below the set peak temperatures. The use of a fired PECVD  $\text{SiN}_x\text{:H}$  surface passivation is known to result in a strong LeTID degradation effect<sup>[26,27]</sup> and was therefore used in this study. The process flow is shown in Figure 1.

Immediately after firing, photoluminescence (PL) images were taken to verify the homogeneity of the samples. To obtain additional information about the spatial homogeneity during the following degradation and regeneration cycle, PL images were taken at selected points, in particular, at maximum degradation and after regeneration.

**Table 1.** Impurity concentrations in the Cz-Si materials under investigation. Dopant concentrations as measured by SIMS and interstitial oxygen data from FTIR measurements.

	B-Reference	B + Al
Dopant concentration [at cm <sup>-3</sup> ]	B: $1.15\text{--}1.2 \times 10^{16}$ Al: $0.3\text{--}0.5 \times 10^{14}$	B: $0.9\text{--}1.1 \times 10^{16}$ Al: $2.8\text{--}3.4 \times 10^{14}$
$\text{O}_i$ [at cm <sup>-3</sup> ]	$6.7 \times 10^{17}$	$7.4 \times 10^{17}$

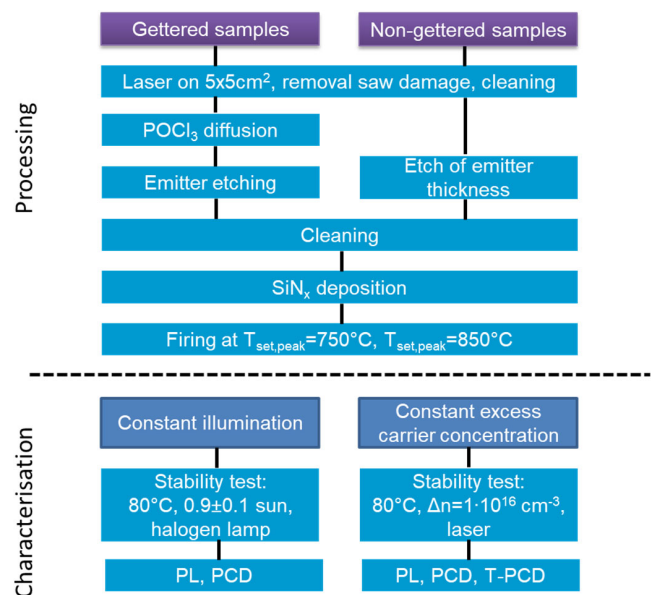


**Figure 1.** Process flow for the gettered and non-gettered samples and subsequent characterization conditions for all samples.

## 2.1. Degradation/Regeneration with Constant Illumination

To investigate the degradation and regeneration behavior, an illumination of  $0.9 \pm 0.1$  suns (halogen lamps) and a treatment temperature of  $80^\circ \text{C}$  on a hotplate were used. The determination of the effective excess charge carrier lifetime  $\tau_{\text{eff}}$  of the samples was done with a Sinton Instruments lifetime tester WCT-120 at  $30^\circ \text{C}$  using the photoconductance decay (PCD) method.<sup>[28]</sup> For the analysis of LeTID/BO-related defect densities, the lifetime measurements were evaluated at an injection of  $\Delta n = 0.1 \times p_0$  (corresponding to an injection of  $1.2 \times 10^{15} \text{ cm}^{-3}$  for the B-Reference and an injection of  $1.1 \times 10^{15} \text{ cm}^{-3}$  for B + Al), with  $p_0$  being the doping density. From  $\tau_{\text{eff}}$ , the change in equivalent defect density  $\Delta N$  was calculated via

$$\Delta N = \frac{1}{\tau_{\text{eff}}(t)} - \frac{1}{\tau_{\text{eff}}(0)} \quad (1)$$

with  $\tau_{\text{eff}}(0)$  and  $\tau_{\text{eff}}(t)$  being the effective lifetime at the start of the experiment and at any given time, respectively.<sup>[25]</sup>

By fitting the equivalent defect density with exponential functions, the effective time constants for degradation and regeneration were determined. In addition to determination of  $\tau_{\text{eff}}$ , the PCD measurements were also be used to determine the values of the surface recombination current density parameter  $j_0$  at high injection (here  $\Delta n = 3 \times 10^{16} \text{ cm}^{-3}$ ) according to the method presented by Kimmerle et al.,<sup>[29,30]</sup> which provides information on the development of surface passivation quality over treatment time.

## 2.2. Degradation/Regeneration with Constant Excess Carrier Concentration

So far, the procedure for constant illumination has been described. However, as  $\tau_{\text{eff}}$  changes over time during

illumination at elevated temperature, injection also changes and this might change the (injection-dependent) reaction rates.<sup>[24,31]</sup>

To investigate whether this dependence had a significant effect on the observed degradation and regeneration kinetics, the comparison between B-Reference and B + Al material was conducted under constant excess carrier concentration conditions. For the measurement with constant excess carrier concentration, the same laser-based setup with a laser beam of 800–805 nm wavelength, as described by Graf et al.,<sup>[24]</sup> was used. During treatment with the laser, the sample was placed on a hotplate at 80 °C. From the individual lifetime measurements, the intensity of the laser was adjusted so that the injection for the following illumination time interval was held constant. For this purpose, a WCT-120TS from Sinton Instruments was used to measure  $\tau_{\text{eff}}$  at treatment temperature (80 °C) to allow adjustment of the laser illumination intensity for the next time step. After each lifetime measurement, the intensity was manually varied on the laser setup, so that the injection under illumination remained almost constant at  $\Delta n \approx 1 \times 10^{16} \text{ cm}^{-3}$ . In addition,  $\tau_{\text{eff}}$  was measured with PCD at 30 °C.

Analogous to the experiment with constant illumination, the evaluation of  $\tau_{\text{eff}}$  and the defect density presented in Results was conducted at  $\Delta n = 0.1 \times p_0$  and at 30 °C.

### 3. Results

The PL images, which are taken immediately after firing, demonstrate that the samples of the two materials are of homogeneous lateral quality and comparable (not shown). The initial  $\tau_{\text{eff}}$  of the materials is in the range of 280–400  $\mu\text{s}$ , as shown in Table 2. As expected, the progression of the measured  $\tau_{\text{eff}}$  values shows a degradation and regeneration behavior, followed by a final reduction in  $\tau_{\text{eff}}$ . For degradation and regeneration, an overlay of boron–oxygen (BO)-related defect kinetics and LeTID is expected.<sup>[24,25,32]</sup>

#### 3.1. Results at Constant Illumination

To compare the changes in degradation and regeneration kinetics between the samples, the defect density  $\Delta N$  is determined via Equation (1). The corresponding defect densities for the differently doped materials are shown in Figure 2, together with the  $j_0$  values. During degradation and at least the early phase of regeneration  $j_0$  does not change, as the observed degradation/regeneration is caused by changes in the Si bulk. This behavior was also already observed by others.<sup>[33]</sup> After the observed regeneration phase (increase in  $\tau_{\text{eff}}$  and decrease in  $\Delta N$ ), there is a further increase in  $\Delta N$  (or decrease in  $\tau_{\text{eff}}$ ) visible, which represents a

**Table 2.** Initial lifetime after firing of the two different materials evaluated at  $\Delta n = 0.1 \times p_0$ .

	B-Reference $\tau_{\text{eff}}(0)$ [ $\mu\text{s}$ ]	B + Al $\tau_{\text{eff}}(0)$ [ $\mu\text{s}$ ]
Non-gettered, $T_{\text{set,peak}} = 750^\circ\text{C}$	286	364
Gettered, $T_{\text{set,peak}} = 750^\circ\text{C}$	406	407
Non-gettered, $T_{\text{set,peak}} = 850^\circ\text{C}$	326	331
Gettered, $T_{\text{set,peak}} = 850^\circ\text{C}$	318	371

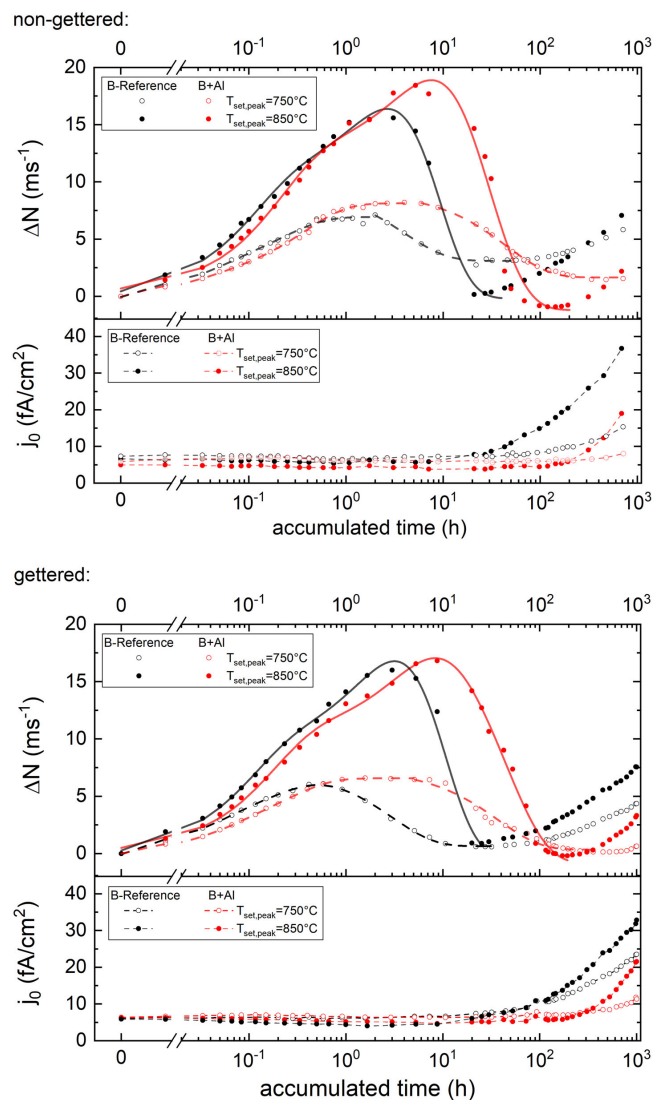


**Figure 2.** Defect density  $\Delta N$  at  $\Delta n = 0.1 \times p_0$  with fit and  $j_0$  over accumulated time at constant illumination for non-gettered (top) and gettered B-Reference and B + Al samples (bottom), fired at two different temperatures. The lines in the graphs correspond to the fit in the case of  $\Delta N$ , and in the case of  $j_0$ , they are a guide to the eye.

surface-related degradation, indicated also by the increasing  $j_0$  (compare, e.g., with Sperber et al.<sup>[33]</sup>).

By fitting the defect density  $\Delta N$ , time constants for degradation and regeneration can be determined, respectively. According to Bredemeier et al.,<sup>[34]</sup> the degradation proceeds in two stages, a fast one followed by a slow degradation. Both stages can be fitted with the sum of two exponential functions.

Here, two exponential functions for degradation and one exponential function for regeneration are used as fitting function.

$$\Delta N(t) = \underbrace{-a_1 \exp\left(-\frac{t}{t_1}\right) - a_2 \exp\left(-\frac{t}{t_2}\right)}_{\text{degradation}} + \underbrace{a_3 \exp\left(-\frac{t}{t_3}\right)}_{\text{regeneration}} + c \quad (2)$$

where  $t_1$  and  $t_2$  are the time constants of degradation,  $t_3$  is the time constant of regeneration, and  $c$  represents the offset. Thereby, the time constants have no directly provable relation to LeTID or BO-LID. The resulting time constants from the fits are shown in Table 3. The uncertainty of the time constants originates from the error of the fits, and the defect density  $\Delta N$  is fitted until the time when  $j_0$  starts to increase.

### 3.1.1. Influence of Gettering

It has been shown by others (e.g., the study by Caballero et al.<sup>[35]</sup>) that gettering can increase  $\tau_{\text{eff}}$  in Cz-Si material and might change the extent of LeTID, especially in mc-Si material (e.g., see other studies<sup>[16,36]</sup>). With the materials used here, the initial lifetime value is slightly higher for almost all gettered samples. Comparing the defect densities  $\Delta N$  of the same material and the same firing temperature, gettering shows no significant influence on degradation and regeneration behavior, possibly due to the lower impurity concentration in Cz-Si as compared with mc-Si. Also, the fit results of the time constants show no significant influence of gettering.

### 3.1.2. Influence of Firing Temperature

As expected for LeTID, firing with higher  $T_{\text{set,peak}}$  results in stronger degradation and leads to higher defect densities.<sup>[24,37]</sup>

For the B-Reference, the comparison of the different firing temperatures shows that for lower  $T_{\text{set,peak}}$  the maximum in  $\Delta N$  is reached faster. This behavior can also be seen in the determined time constants, where  $t_1$  and  $t_2$  at  $T_{\text{set,peak}} = 750^\circ\text{C}$  are smaller than for  $850^\circ\text{C}$ . However, the time of reaching the following minimum in  $\Delta N$  is very similar for both firing temperatures. For the B + Al case, the behavior concerning firing temperature is different. It can be seen from the results of  $t_1$  and  $t_2$  that at lower  $T_{\text{set,peak}}$  the maximum is reached faster too. However, the following minimum in  $\Delta N$  is delayed at lower

firing temperatures. Also, at lower firing temperature, a plateau is visible around the  $\Delta N$  maximum, which is not present at higher firing temperature.

The increase in  $j_0$  values is more pronounced at higher firing temperatures, which could be due to the increased diffusion of hydrogen from the passivation layer due to the higher temperature.

### 3.1.3. Influence of Dopant

In addition to the influence of gettering and firing temperature, the main focus of this article is to investigate the effect of addition of Al on the observable degradation/regeneration kinetics. The degradation kinetics of the B-Reference and B + Al samples are almost the same up to the  $\Delta N$  maximum of the B-Reference. Especially at the lower firing temperature, it can be seen for the B + Al samples that when the  $\Delta N$  maximum is reached, the value remains almost constant for a certain period of time before regeneration sets in.

A particular aspect in the comparison is the observed delay in the onset of regeneration for the B + Al materials compared to the B-Reference. The regeneration for the B-Reference sets in after 1–5 h and the  $\Delta N$  minimum is reached after about 20–30 h, whereas for B + Al, the regeneration starts after 3–8 h and the  $\Delta N$  minimum is reached only at >120 h.

For the two materials the time constants  $t_1$  and  $t_2$  are in the same order of magnitude, which indicate that there is no significant change in the degradation kinetics of the B + Al compared with the B-Reference samples. In the case of regeneration, the time constants  $t_3$  for the B + Al samples are about 5–10 times higher than for the B-Reference, confirming a significant delay in regeneration compared with B-Reference.

Figure 2 shows a delayed increase in  $j_0$  values for B + Al compared with the B-Reference samples. Assuming that the course of  $j_0$  corresponds to a saturating increase, which can be described by an exponential function, the delayed increase in B + Al could also be attributed to a smaller amplitude at the same time constant. So it seems that B + Al has an influence on surface degradation, either by the amplitude or the time constant. As the passivation layer is the same for both materials, the presence of Al in the B + Al material apparently causes the change of the surface-related degradation.

**Table 3.** Resulting time constants for degradation ( $t_1$ ,  $t_2$ ) and regeneration ( $t_3$ ) of the differently doped materials by fitting the defect density  $\Delta N$  obtained at constant illumination. The numbers in brackets correspond to the uncertainty of the time constants from the fit.

		B-Reference [h]	B + Al [h]
Non-gettered; $T_{\text{set,peak}} = 750^\circ\text{C}$	$t_1$	0.04(1)	0.03(1)
	$t_2$	0.23(3)	0.38(3)
	$t_3$	4.0(5)	46.1(15)
Gettered; $T_{\text{set,peak}} = 750^\circ\text{C}$	$t_1$	0.04(1)	0.05(1)
	$t_2$	0.20(3)	0.26(1)
	$t_3$	3.0(2)	37.7(29)
Non-gettered; $T_{\text{set,peak}} = 850^\circ\text{C}$	$t_1$	0.11(1)	0.21(5)
	$t_2$	2.7(8)	5.9(11)
	$t_3$	5.7(13)	25.0(46)
Gettered; $T_{\text{set,peak}} = 850^\circ\text{C}$	$t_1$	0.08(1)	0.17(2)
	$t_2$	0.67(7)	4.5(8)
	$t_3$	6.3(24)	43.9(38)

## 3.2. Results at Constant Excess Carrier Concentration

To check whether the observed behavior is injection dependent, the two materials under investigation are treated at constant excess carrier concentration, too.

The results on the influence of gettering and firing temperature are equivalent to the results with constant illumination. Therefore, the focus here lies on the influence of Al addition on the observed degradation/regeneration kinetics and the time delay of the regeneration.

Figure 3 shows the resulting defect density  $\Delta N$  and  $j_0$  values for the gettered and non-gettered samples fired at  $850^\circ\text{C}$ .

Although the delay of regeneration is less pronounced compared with the treatment conditions at constant illumination for samples fired at  $850^\circ\text{C}$ , the effect is still significant.



Furthermore, the degradation kinetics are almost the same for the two materials up to the  $\Delta N$  maximum of the B-Reference. However, the degradation kinetics have changed as, unlike for the previous investigation, the use of only one exponential function is sufficient for fitting the degradation with very good accuracy.

The defect densities  $\Delta N$  are fitted with the function

$$\Delta N(t) = \underbrace{-a_1 \exp\left(-\frac{t}{t_1}\right)}_{\text{degradation}} + \underbrace{a_3 \exp\left(-\frac{t}{t_3}\right)}_{\text{regeneration}} + c \quad (3)$$

where  $t_1$  and  $t_3$  are the time constants for the degradation and regeneration, respectively, and  $c$  represents the offset. The resulting time constants of the fits are shown in Table 4.

As for the experiment with constant illumination, the degradation constants for both materials do not differ significantly.

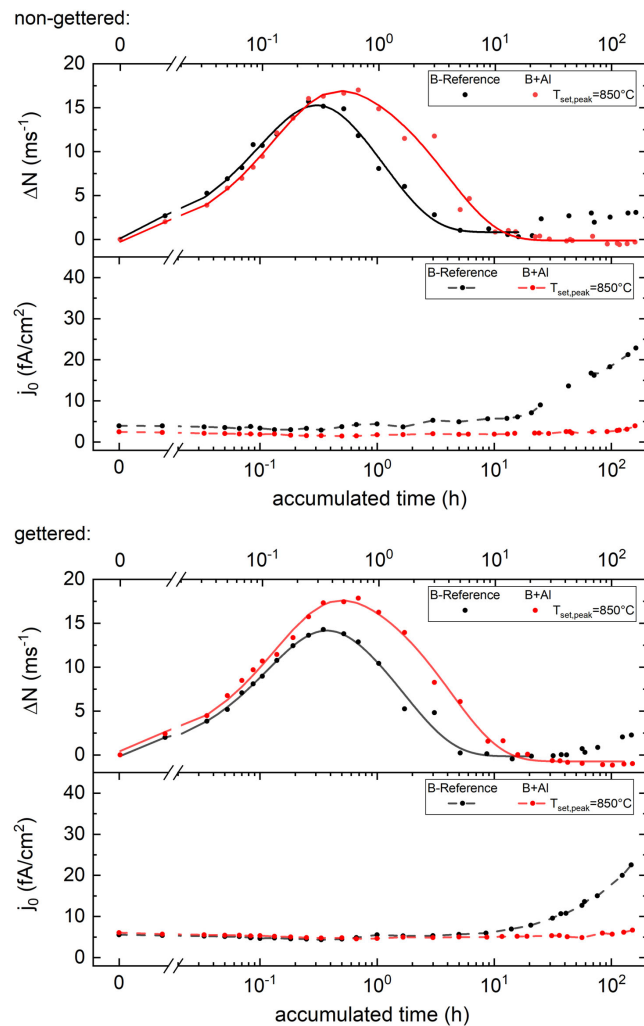


**Figure 3.** Defect density  $\Delta N$  at  $\Delta n = 0.1 \times p_0$  with fit and  $j_0$  values over accumulated time at constant excess carrier concentration for non-gettered (top) and gettered B-Reference and B + Al samples (bottom) fired at 850 °C. The lines in the graphs correspond to the fit in the case of  $\Delta N$ , and in the case of  $j_0$  they are a guide to the eye.

Compared with constant illumination, the time constant of regeneration for B + Al fired at  $T_{\text{set,peak}} = 850$  °C is now only a factor of 2–4 higher than for the B-Reference. As the delay of regeneration at constant excess carrier concentration is less pronounced than for the treatment at constant illumination, the underlying mechanism causing this effect seems to be injection dependent. Interestingly, the delayed onset of regeneration leads to a higher maximum  $\Delta N$  value (compared with results of Wagner et al.<sup>[23]</sup>). Within the treatment period, the  $j_0$  values for B + Al do not yet start to increase or at least are hardly noticeably, whereas for the B-Reference, the  $j_0$  values are already increasing. Thus, the increase in  $j_0$  for B + Al is also delayed here.

Compared with the experiment at constant illumination, both degradation and regeneration are sped up as both processes are known to be dependent on injection.<sup>[24]</sup>

## 4. Discussion

To find possible causes for the delay in regeneration of the B + Al samples, factors such as the dopant itself and the influence of O and H as possible partners interacting with the dopant are considered in the following paragraphs.

As B concentration is very similar for all materials under investigation, all other experimental conditions are kept as constant as possible and only the Al concentration differs by an order of magnitude in both materials, the differences in long-term  $\tau_{\text{eff}}$  or  $\Delta N$  behavior, respectively, seem to originate from the presence of more Al atoms. The Al content could in principle influence both the degradation and the regeneration behavior, but from the presented results, the influence on regeneration seems to be much more significant. This can be directly seen from the determined time constants, where the time constants of degradation are comparable for both materials. According to Huster et al.<sup>[38]</sup> and Steinkemper et al.,<sup>[39]</sup> an incomplete ionization of Al is highly unlikely for a doping concentration below  $N_d \approx 10^{18} \text{ cm}^{-3}$ . Therefore, the Al dopant atoms can be considered as completely ionized due to the lower dopant concentration in the materials.

The effect of BO-LID is more pronounced relatively compared with LeTID at lower firing temperatures.<sup>[24,40]</sup> Thus, the relative effect of BO-LID at  $T_{\text{set,peak}} = 850$  °C is lower and the observed behavior is more dominated by LeTID. As regeneration delays occur at both firing temperatures, Al appears to slow down

**Table 4.** Resulting time constants for degradation ( $t_1$ ) and regeneration ( $t_3$ ) of the differently doped materials by fitting the defect density  $\Delta N$  obtained at constant excess carrier concentration ( $\Delta n \approx 10^{16} \text{ cm}^{-3}$ ). The numbers in brackets correspond to the uncertainty of the time constants from the fit.

		B-Reference [h]	B + Al [h]
Non-gettered; $T_{\text{set,peak}} = 850$ °C	$t_1$	0.12(1)	0.13(1)
	$t_3$	1.1(1)	3.9(3)
Gettered; $T_{\text{set,peak}} = 850$ °C	$t_1$	0.13(1)	0.14(1)
	$t_3$	1.6(2)	4.2(3)

the LeTID regeneration process, but an additional delay in BO regeneration cannot be excluded.

Besides boron, oxygen could also combine with Al. However, according to Schmidt et al.,<sup>[41]</sup> the AlO-related complex forms mainly at high temperatures  $>900^\circ\text{C}$ . As the firing temperature is too low, it is unclear how relevant the AlO-related complex is in the samples. In principle, it could have formed already during crystallization, but as the starting  $\tau_{\text{eff}}$  is similar for both B-Reference and B + Al, we think that it can be neglected in the discussion.

In addition to the dopant, hydrogen in particular plays an important role in long-term lifetime behavior. The binding energy for Al–H of  $E_b = 1.44 \pm 0.03$  eV is higher than that for B–H ( $1.28 \pm 0.03$  eV).<sup>[42]</sup> Therefore, during regeneration, the breaking of the Al–H bonds may be more unlikely due to the higher binding energy, resulting in a longer average time for release. However, note that the binding energy (or more precisely the activation energy for the release process of H) should be known under treatment conditions (injection), as there are hints that this energy is different from the value in the dark (possibly due to charge effects),<sup>[43]</sup> and the binding energies in the study by Zundel and Weber<sup>[42]</sup> were measured in the dark.

It was reported in literature that regeneration of BO-LID might be triggered by dissolution of BH pairs.<sup>[44]</sup> Therefore, the presence of AlH pairs with higher activation energy for release of H could be responsible for a delayed BO-LID regeneration. As LeTID seems to be the dominant phenomenon for the samples fired at  $850^\circ\text{C}$ , Al seems to affect the LeTID regeneration kinetics, too. Under the assumption that H is involved in the LeTID formation and/or regeneration process,<sup>[15,20,21,36,45]</sup> and the activation energy to release H from Al is higher than for releasing it from B as acceptors in c-Si, the following model can be formulated: During the regeneration process the presence of “free” H is necessary that was formerly “stored” or attached to the acceptor atoms. The “freeing” of H from the dopant H configuration takes longer for Al–H in average and slows down the regeneration process. Whether this “free” H is atomic or in another configuration is not clear yet, although some models exist (e.g., see the study by Voronkov et al.<sup>[46]</sup>). Although the Al concentration is much smaller than the B concentration, the Al atoms still might have a significant impact, as only around  $10^{14}\text{ cm}^{-3}$  H atoms are bound to the acceptor after a typical firing step,<sup>[47]</sup> and release and retrapping of H at acceptors might occur frequently, resulting in a higher chance that H ends up at an Al atom due to the higher activation energy for release.

The dependence of LeTID regeneration on the presence of “free” H might also have implications to explain the observed differences in LeTID kinetics for different p-type Si materials. LeTID kinetics seem to be slower in mc-Si as compared with Cz-Si.<sup>[8,9]</sup> One explanation in accordance with the introduced model might be the fact that there are less traps for H in Cz-Si, but the concentration of defects (and therefore possible locations of traps for H) is much higher in mc-Si, slowing down the effective diffusion constant of H (compare, e.g., with strongly varying effective hydrogen diffusion constants presented by Kleekajai et al.<sup>[48]</sup>). However, it has to be stated that a comparison of LeTID kinetics should be done at the same and constant excess

carrier concentration conditions for all materials due to the injection dependency of the reaction rates, and not at constant illumination, as it is usually done.

The  $j_0$  values show a delayed increase in the case of B + Al. As H has an influence on LeTID and both, regeneration as well as onset of surface-related degradation are delayed for B + Al, both effects might be caused by the same mechanism, a reduced effective diffusion of H. If true, then the observed loss of surface passivation quality would be caused by H from the silicon bulk reaching the surface region. Whether the degradation is caused by excess concentration of H, or H changing its configuration (or diffusing out of the sample), is still unclear.

By treating the samples at constant excess carrier concentration, it was shown that the effect is injection dependent. For the determination of the time constant of degradation, only one exponential function is sufficient, indicating that the need for two exponential fitting functions in the case of constant illumination might be due to the change in  $\tau_{\text{eff}}$  over treatment time and the time constant depending on (in this case not constant) injection.

The influence of Al on LeTID could not only be shown on Cz-Si lifetime samples. First experiments showed that the time delay in B + Al can also be observed in mc-Si lifetime samples at different degradation temperatures and also in mc- and Cz-PERC solar cells at the same degradation conditions as used here (not shown in this work). Yet the effect is less pronounced in the mc wafers, as other defects may also play a role.

## 5. Conclusion and Outlook

It could be shown that addition of aluminum in boron-doped Cz-Si leads to a time delay in the observed regeneration kinetics. In the case of the B + Al material, the fitted time constants of regeneration at constant generation are about a factor of 5–10 higher than for the B-Reference. As the delay is still significant, but less pronounced in the investigation with constant excess carrier concentration, the effect causing the delay seems to be injection dependent. Higher firing temperatures lead to higher defect concentrations as expected, but gettering does not show a significant effect on the observed kinetics.

By measuring the  $j_0$  values, it was possible to show in the case of B + Al material that its increase is delayed, too.

A model is proposed that might explain both observed effects. A higher activation energy for splitting Al–H pairs as compared with B–H pairs results in a delayed “freeing” of H from dopant H configuration. This would indicate that the observed regeneration is dependent on this “freed” H which might also be responsible for degradation of surface passivation once reaching the sample surface. The exact mechanism of surface-related degradation is not yet clear.

Further experiments with the comparisons of differently contaminated Si materials can further examine the influence of the dopants on degradation and regeneration and are currently under way.

## Acknowledgements

The authors would like to thank Axel Herguth and Frank Huster for instructive discussions and explanations. Part of this work was funded by the German BMWi under contract 03EE1051. The content is the responsibility of the authors.

Open access funding enabled and organized by Projekt DEAL.

## Conflict of Interest

The authors declare no conflict of interest.

## Data Availability Statement

Research data are not shared.

## Keywords

aluminum, Czochralski-grown Si, defect densities, degradations, lifetimes, light- and elevated temperature-induced degradation, regenerations

Received: September 6, 2021

Revised: September 27, 2021

Published online: October 13, 2021

- [1] H. Fischer, W. Pschunder, in *Conf. Record 10<sup>th</sup> Photovoltaic Specialists Conf.*, IEEE, New York, NY **1973**, pp. 404–411.
- [2] S. W. Glunz, S. Rein, W. Warta, J. Knobloch, W. Wettling, *Sol. Energy Mater. Sol. Cells* **2001**, *65*, 219.
- [3] S. Rein, S. Diez, R. Falster, S. W. Glunz, in *Proc. of the 3rd WCPEC, WCPEC-3 Organising Committee*, Arisumi Printing Inc., Osaka, Japan **2003**, pp. 1048–1052.
- [4] K. Bothe, R. Sinton, J. Schmidt, *Prog. Photovoltaics Res. Appl.* **2005**, *13*, 287.
- [5] A. Herguth, G. Schubert, M. Kaes, G. Hahn, in *Conf. Record of the 2006 IEEE 4<sup>th</sup> World Conf. on Photovoltaic Energy Conversion*, Vol. 1, IEEE, New York, NY **2006**, pp. 940–943.
- [6] S. Wilking, A. Herguth, G. Hahn, *J. Appl. Phys.* **2013**, *113*, 194503.
- [7] A. Herguth, B. Hallam, *AIP Conf. Proc.* **2018**, *1999*, 130006.
- [8] K. Ramspeck, S. Zimmermann, H. Nagel, A. Metz, Y. Gassenbauer, B. Birkmann, A. Seidl, in *Proc. 27<sup>th</sup> European Photovoltaic Solar Energy Conf. and Exhibition*, WIP Renewable Energies, München, Germany **2012**, pp. 861–865.
- [9] F. Kersten, P. Engelhart, H. C. Ploigt, A. Stekolnikov, T. Lindner, F. Stenzel, M. Bartzsch, A. Szpeth, K. Petter, J. Heitmann, J. W. Müller, *Sol. Energy Mater. Sol. Cells* **2015**, *142*, 83.
- [10] J. Fritz, A. Zuschlag, D. Skorka, A. Schmid, G. Hahn, in *Proc. 33<sup>rd</sup> European Photovoltaic Solar Energy Conf. and Exhibition*, WIP Renewable Energies, München, Germany **2017**, pp. 569–572.
- [11] F. Kersten, P. Engelhart, H.-C. Ploigt, F. Stenzel, K. Petter, T. Lindner, A. Szpeth, M. Bartzsch, A. Stekolnikov, M. Scherff, J. Heitmann, J. W. Müller, in *Proc. 31<sup>st</sup> European Photovoltaic Solar Energy Conf. and Exhibition*, WIP Renewable Energies, München, Germany **2015**, pp. 1830–1834.
- [12] C. Vargas Castrillon, K. Kim, G. Coletti, D. Payne, C. Chan, S. R. Wenham, Z. Hameiri, in *Proc. 33<sup>rd</sup> European Photovoltaic Solar Energy Conf. and Exhibition*, WIP Renewable Energies, München, Germany **2017**, pp. 561–564.
- [13] D. Chen, P. Hamer, M. Kim, C. Chan, A. C. Nee Wenham, F. Rougieux, Y. Zhang, M. Abbott, *Sol. Energy Mater. Sol. Cells* **2020**, *207*, 110353.
- [14] D. Bredemeier, D. Walter, S. Herlufsen, J. Schmidt, *AIP Adv.* **2016**, *6*, 035119.
- [15] R. Eberle, W. Kwapil, F. Schindler, M. C. Schubert, S. W. Glunz, *Phys. Status Solidi RRL* **2016**, *10*, 861.
- [16] D. Skorka, A. Zuschlag, G. Hahn, *AIP Conf. Proc.* **2018**, *1999*, 130015.
- [17] D. Bredemeier, D. C. Walter, J. Schmidt, *Solar RRL* **2018**, *2*, 1700159.
- [18] M. A. Jensen, A. Zuschlag, D. Skorka, S. Wieghold, A. E. Morishige, G. Hahn, T. Buonassisi, *J. Appl. Phys.* **2018**, *124*, 085701.
- [19] J. Schmidt, D. Bredemeier, D. C. Walter, *IEEE J. Photovoltaics* **2019**, *9*, 1497.
- [20] A. Schmid, C. Fischer, D. Skorka, A. Herguth, C. Winter, A. Zuschlag, G. Hahn, *IEEE J. Photovoltaics* **2021**, *11*, 967.
- [21] K. Nakayashiki, J. Hofstetter, A. E. Morishige, T.-T. A. Li, D. B. Needleman, M. A. Jensen, T. Buonassisi, *IEEE J. Photovoltaics* **2016**, *6*, 860.
- [22] M. A. Jensen, A. E. Morishige, J. Hofstetter, D. B. Needleman, T. Buonassisi, *IEEE J. Photovoltaics* **2017**, *7*, 980.
- [23] M. Wagner, F. Wolny, M. Hentsche, A. Krause, L. Sylla, F. Kropfgans, M. Ernst, R. Zierer, P. Bönsch, P. Müller, N. Schmidt, V. Osinniy, H.-P. Hartmann, R. Mehnert, H. Neuhaus, *Sol. Energy Mater. Sol. Cells* **2018**, *187*, 176.
- [24] A. Graf, A. Herguth, G. Hahn, *AIP Conf. Proc.* **2019**, *2147*, 140003.
- [25] A. Herguth, *IEEE J. Photovoltaics* **2019**, *9*, 1182.
- [26] F. Kersten, J. Heitmann, J. W. Müller, *Energy Procedia* **2016**, *92*, 828.
- [27] J. Lindroos, A. Zuschlag, D. Skorka, G. Hahn, *IEEE J. Photovoltaics* **2019**, *10*, 8.
- [28] R. A. Sinton, A. Cuevas, *Appl. Phys. Lett.* **1996**, *69*, 2510.
- [29] A. Kimmeler, J. Greulich, A. Wolf, *Sol. Energy Mater. Sol. Cells* **2015**, *142*, 116.
- [30] D. E. Kane, R. M. Swanson, in *Conf. Record 18<sup>th</sup> Photovoltaic Specialists Conf.*, IEEE, New York, NY **1985**, pp. 578–583.
- [31] D. C. Walter, L. Helmich, D. Bredemeier, R. Falster, V. V. Voronkov, J. Schmidt, in *Proc. 35<sup>th</sup> European Photovoltaic Solar Energy Conf. and Exhibition*, WIP Renewable Energies, München, Germany **2018**, pp. 522–526.
- [32] A. Herguth, in *Conf. Record 46<sup>th</sup> Photovoltaic Specialists Conf.*, IEEE, New York, NY **2019**, pp. 54–60.
- [33] D. Sperber, A. Graf, D. Skorka, A. Herguth, G. Hahn, *IEEE J. Photovoltaics* **2017**, *7*, 1627.
- [34] D. Bredemeier, D. Walter, J. Schmidt, *Sol. Energy Mater. Sol. Cells* **2017**, *173*, 2.
- [35] L. J. Caballero, C. Del Cañizo, P. Sanchez-Friera, A. Luque, *Sol. Energy Mater. Sol. Cells* **2005**, *88*, 247.
- [36] A. Zuschlag, D. Skorka, G. Hahn, *Prog. Photovolt. Res. Appl.* **2017**, *25*, 545.
- [37] T. Niewelt, M. Selinger, N. E. Grant, W. Kwapil, J. D. Murphy, M. C. Schubert, *J. Appl. Phys.* **2017**, *121*, 185702.
- [38] F. Huster, G. Schubert, in *Proc. 20<sup>th</sup> European Photovoltaic Solar Energy Conf. and Exhibition*, WIP Renewable Energies, München, Germany **2005**, pp. 1462–1465.
- [39] H. Steinkemper, M. Rauer, P. Altermatt, F. D. Heinz, C. Schmiga, M. Hermle, *J. Appl. Phys.* **2015**, *117*, 074504.
- [40] D. Chen, M. Kim, B. V. Stefani, B. J. Hallam, M. D. Abbott, C. E. Chan, R. Chen, D. N. Payne, N. Nampalli, A. Ciesla, T. H. Fung, K. Kim, S. R. Wenham, *Sol. Energy Mater. Sol. Cells* **2017**, *172*, 293.
- [41] J. Schmidt, N. Thiemann, R. Bock, R. Brendel, *J. Appl. Phys.* **2009**, *106*, 9.
- [42] T. Zundel, J. Weber, *Phys. Rev. B* **1989**, *39*, 13549.

- [43] T. Zundel, J. Weber, *Phys. Rev. B* **1991**, 43 4361.
- [44] S. Wilking, C. Beckh, S. Ebert, A. Herguth, G. Hahn, *Sol. Energy Mater. Sol. Cells* **2014**, 131, 2.
- [45] T. H. Fung, M. Kim, D. Chen, C. Chan, B. Hallam, R. Chen, D. Payne, A. Ciesla, S. Wenham, M. Abbott, *Sol. Energy Mater. Sol. Cells* **2018**, 184, 48.
- [46] V. V. Voronkov, R. Falster, *Phys. Status Solidi B* **2017**, 254, 1600779.
- [47] C. Winter, J. Simon, A. Herguth, *Phys. Status Solidi A* **2021**, 2100220.
- [48] S. Kleekajai, F. Jiang, M. Stavola, V. Yelundur, K. Nakayashiki, A. Rohatgi, G. Hahn, S. Seren, J. Kalejs, *J. Appl. Phys.* **2006**, 100, 093517.